Available online at www.sciencedirect.com

ScienceDirect

Ceramics International 38S (2012) S585–S588

CERAMICS INTERNATIONAL

www.elsevier.com/locate/ceramint

Infra-red emission properties of ZnO:Er thin films prepared on the sapphire substrates

Jun Seong Lee, Young Jin Kim *

Department of Materials Science and Engineering, Kyonggi University, Suwon 443-760, Republic of Korea

Available online 27 May 2011

Abstract

ZnO thin films with various Er content were deposited on *c*-plane sapphire substrates by rf magnetron sputtering. As deposited-films showed poor crystallinity due to the strains induced in the films, but the well-developed (0 0 2) preferred films could be achieved after post-annealing under air atmosphere. X-ray diffraction patterns of 5 and 10 mol% Er_2O_3 doped ZnO films exhibited the un-reacted Er_2O_3 phase, which were possibly located at the grain boundaries. The emission spectra of ZnO:Er films pumped by 515 nm laser showed infrared emissions at 1.538 μm due to the energy transition between $^4I_{13/2}$ and $^4I_{15/2}$ of Eu^{3+} ions. IR emission behaviors strongly correlated with the film structure.

Keywords: A. Films; C. Optical properties; D. ZnO; E. Functional applications

1. Introduction

Er-doped semiconductor materials such as GaN, GaAs, and Si have been of interest for the optical applications ranging from visible to infrared (IR) region [1–3]. To improve 1.54 μm IR emission properties, it is known that oxygen co-doped and wide-band gap semiconductors are more effective [4,5]. For this purpose Er-doped ZnO has been attractive due to the wide band-gap (~3.3 eV) and coexistence of Er and O.

Komuro et al. have intensively investigated IR emission dynamics of ZnO:Er thin films prepared on quartz substrates by a laser ablation method [6,7]. They showed that the rise time of 1.54 μm emission of ZnO:Er films under the indirect excitation (a carrier-mediated process in ZnO host) was shorter than that under the direct pumping into the 4f energy level of the Er^{3+} ions, while the 1.54 μm emission spectrum feature did not change. This demonstrated that the indirect excitation was superior to the direct excitation in the excitation efficiency. It is known that the crystal field coordinated by the octahedral oxygen ions with a low symmetry is more desirable for the intra-4f transition of Er^{3+} ions. Ishii et al. reported that a pseudo-octahedral structure with C_{4v} symmetry, which was similar to Er-doped Si, could be obtained by annealing under O_2 atmosphere, leading to the strong 1.54 μm emission [8,9]. Another way to achieve a locally distorted structure surrounding oxygen ions is adding some impurities. The substitution of N or Li, for instance, contributed to the distortion of a local symmetry and the crystal structure around Er^{3+} ions, resulting in the increase in PL intensity of ZnO:Er powders [10].

The crystallinity of ZnO thin films also affects the PL properties. It was suggested that (0 0 2) epitaxial ZnO:Er films could be achieved on *c*-plane sapphire substrates, which showed the strong 1.54 μm Er emissions by minimizing the Er segregations at the grain boundaries as well as providing the well arranged crystal-field around the Er-atoms in ZnO [11].

In this work, ZnO thin films were prepared by a rf magnetron sputtering, and then the effects of Er concentrations on the growing behaviors and the infrared emissions of ZnO:Er thin films were investigated.

2. Experimental

Erbium ions doped ZnO thin films were deposited on *c*-plane sapphire substrates (2 inch diameter, Crystal-on Co., Ltd.) by rf magnetron sputtering. Ar and O_2 gases were introduced together into the chamber as a sputtering gas and an oxidant, respectively. The oxygen partial pressure [O_2/(O_2 + Ar)], the substrate temperature, and rf power were fixed at 50%, 300 °C,

* Corresponding author. Tel.: +82 31 249 9766; fax: +82 31 244 6300.
E-mail address: yjkim@kyonggi.ac.kr (Y.J. Kim).

0272-8842/$36.00
doi:10.1016/j.ceramint.2011.05.103

and 100 W, respectively. These optimum parameters were determined according to our previous work [11]. ZnO:Er ceramic targets were fabricated by a conventional ceramic process, pressing the mixture of ZnO (High Purity Chemicals, 99.999%) and Er_2O_3 powder (United International Inc., 99.9%) in 3 inch diameter molder and sintering it at 1100 °C for 3 h under air atmosphere. The compositional ratios of Er_2O_3 to ZnO were 0, 1, 3, 5, and 10 mol%. Thin films were post-annealed in the tube furnace for 3 h at 700 °C under air atmosphere. All samples had the same thickness of 2 μm by controlling the deposition time.

The structural properties of the films were determined using X-ray diffractometer (XRD, PHILIPS X'pert) $\theta - 2\theta$ scan with Cu Kα radiation (λ = 1.5405 Å). Scanning angle and speed were 20–70° and 5°/s, respectively. Field emission scanning electron microscope (FESEM, JEOL JSM-6500F) was used to observe the surface morphology and to measure the film thickness. The determination of Zn/Er atomic ratio (±10%) was performed at 3 points in each film by an energy dispersive spectroscopy (EDS, JEOL JSM-6500F), and its error range was less than ±10%. Samples were pumped by Coherent Innova Ar laser and IR emissions were detected by Hammamatsu InGaAs diode.

3. Results and discussion

ZnO:Er sputtering targets were fabricated with various Er_2O_3 content (0, 1, 3, 5, and 10 mol%), and the deposited films from each target are referred to as ZO, EZO(1), EZO(3), EZO(5), and EZO(10), respectively. With increasing Er_2O_3 content in the sputtering targets the deposition rate steeply decreases as shown in Fig. 1. The deposition rate (±10%) was obtained by dividing the films thickness by the deposition time, 2 h. The sintered sputtering target of pure ZnO was very dense, whereas the increase in the Er_2O_3 content in the sputtering targets caused the poor density, leading to the low deposition rate.

The variation of Er/Zn atomic ratio (R_A) is shown in Fig. 2. R_A values of the sputtering targets are in just accordance with calculated ones if the measuring errors (10%) are considered. However, the deposited films exhibited higher R_A values

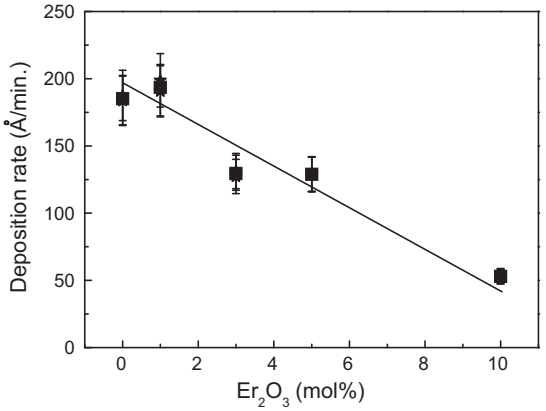

Fig. 1. The deposition rate as a function of the Er_2O_3 content.

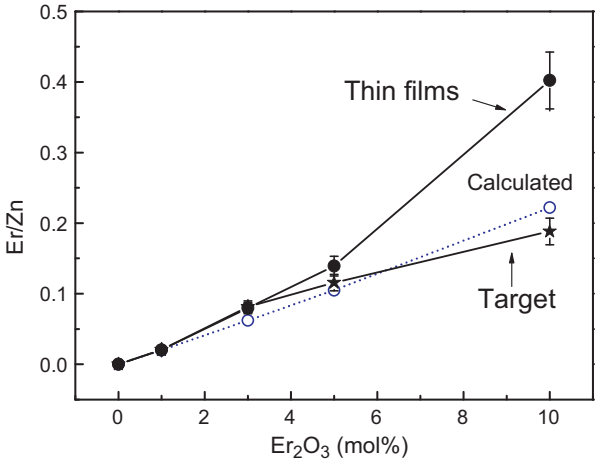

Fig. 2. The Er/Zn atomic ratios of films as a function of the Er_2O_3 content.

comparing with them. This indicated that Er atoms arrived onto the substrates more than Zn atoms during a sputtering. The most possible reasons is scattering angle difference in sputtered atoms, which are attributed to the different atomic weight (Er: 167.26, Zn: 65.38). The heavier sputtered atoms (Er) have lower scattering angles after the collisions, resulting in more incident flux onto the substrates comparing to the lighter ones (Zn) [12].

XRD patterns of as-deposited and post-annealed ZnO:Er thin films are shown in Fig. 3. It is well-known that the crystalline ZnO thin films deposited on *c*-plane sapphire substrates exhibit (0 0 2) preferred characteristic peak at 34.4°. However, as-deposited ZnO:Er thin films in this work show broad and weak peaks at lower angles, indicating the poor crystallinity that possibly originates from the stress due to the thick films of 2 μm. After post-annealing, the stress of as-deposited films was relaxed and also the atoms were rearranged because of the thermal energy, resulting in the well-developed (0 0 2) preferred orientation at 34.4°. In pure ZnO, (0 0 2) peak strongly appears, but it becomes weaker and broader with increasing Er content. Un-reacted Er_2O_3 peak begins to be observed in EZO(5) and then strongly appears in EZO(10),

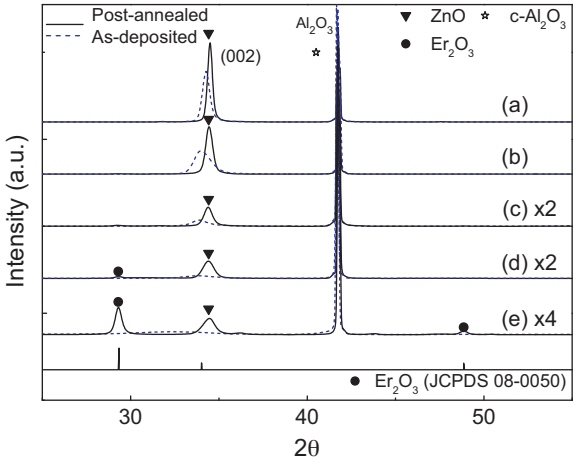

Fig. 3. XRD patterns of ZnO:Er thin films. (a) Pure ZnO, (b) 1 mol%, (c) 3 mol%, (d) 5 mol%, and (e) 10 mol% Er_2O_3.

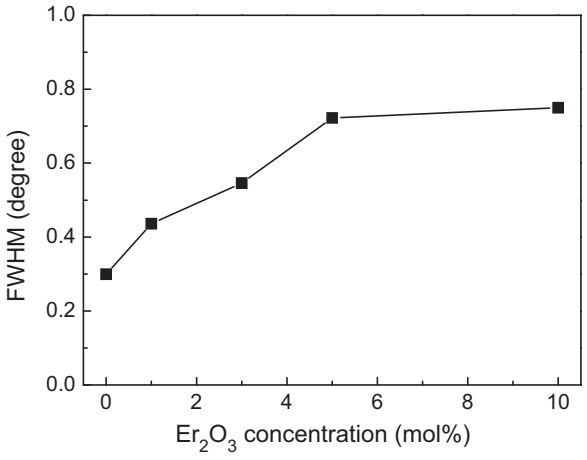

Fig. 4. FWHM of (0 0 2) peak of ZnO:Er films with various Er_2O_3 content.

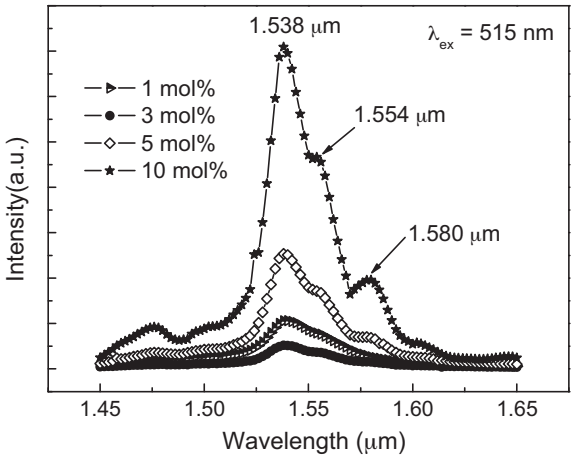

Fig. 6. IR emission spectra of ZnO:Er thin films under 515 nm excitation.

whereas it is not shown in EZO(3). This demonstrated that Er atoms were completely incorporated in the ZnO lattice in EZO(1) and EZO(3) samples, but the further addition of Er_2O_3 caused the un-reacted Er_2O_3 phase in EZO(5) and EZO(10), which might segregate at the grain boundaries.

Er ions incorporated in the ZnO lattice led to the lattice distortion due to the large ionic radius (Er: ~1.03 Å, Zn: ~0.88 Å), and acted as grain growth inhibitors, decreasing the crystallinity. Furthermore excess Er atoms in EZO(5) and EZO(10) prefer to be located at the grain boundaries, inhibiting ZnO films from the (0 0 2) preferred growing [2]. Similar results were reported in the deposition of ZnO:Al [13,14]. The excess Al doping concentration above the critical point caused the stress due to the difference in the ionic size and the segregation of dopants at the grain boundaries, deteriorating the crystallinity. The variation of the crystallinity can be verified by measuring FWHM (full width at half maximum) of (0 0 2) peak as shown in Fig. 4. FWHM of ZnO films continuously increases up to 5 mol% Er_2O_3, and then saturates at above. This result demonstrated that the crystallinity was deteriorated by the increase in the Er_2O_3 content, and was matched well with Fig. 3. SEM micrographs are shown in Fig. 5. Well-developed surface morphology is observed in pure ZnO, while adding Er_2O_3 make the grain smaller, resulting in the very smooth surface in EZO(10).

Fig. 6 exhibits the PL emission spectra excited by 515 nm of ZnO:Er films after post-annealing under air atmosphere, whereas the PL spectra of as-deposited films is too poor to be measured. A peak wavelength at 1.538 μm is assigned to the energy transition of the first excited state ($^4I_{13/2}$) to the ground state ($^4I_{15/2}$) in the Er^{3+} ions incorporated in ZnO lattice [6]. Post-annealing effects can be explained by the local structure of an optically active center in the films [7,9,11]. The 4f-intra transitions of Er are suppressed because of the high-order coordination of O as well as the low symmetry configuration surrounding Er^{3+} ions, resulting in the low PL intensity. However, PL emission can be significantly promoted by post-annealing under air atmosphere, because the diffusion of excess oxygen from the air atmosphere changes the local structure, resulting in a pseudo-octahedral structure with C_{4v} symmetry.

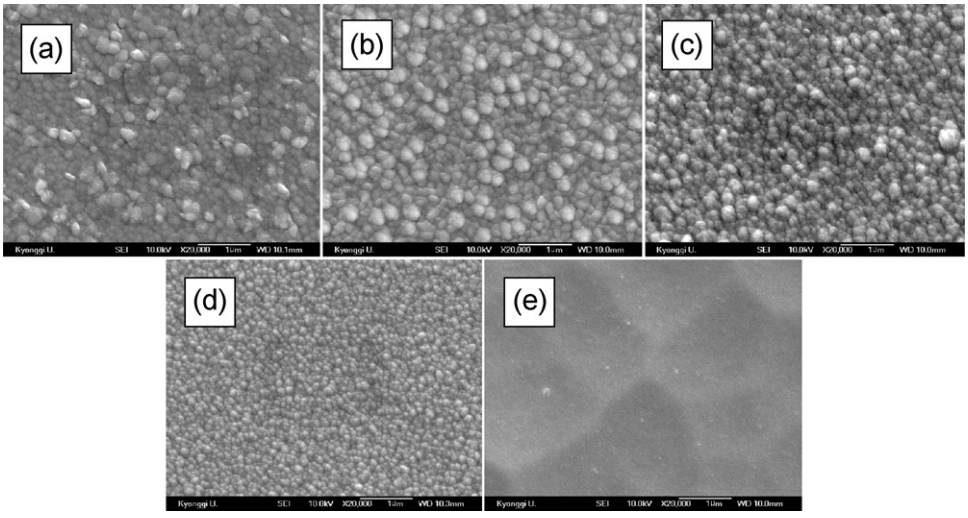

Fig. 5. SEM micrographs of ZnO:Er thin films. (a) Pure ZnO, (b) 1 mol%, (c) 3 mol%, (d) 5 mol%, and (e) 10 mol% Er_2O_3.

EZO(1) is superior to EZO(3) in the emission intensity in spite of the low Er content, while the crystallinity of EZO(1) is better than that of EZO(3) as shown in Fig. 4. This result suggests that the higher crystallinity contributes to the enhanced emission more than the higher Er content. Namely, the highly ordered crystal-field surrounding Er atoms in ZnO films are quite effective. Meanwhile the broad spectra of EZO(1) and EZO(3) show the apparent evidence that the strains are induced in the films due to the difference in valence and size between Er^{3+} and Zn^{2+} ions. However, with increasing Er_2O_3 content above 5 mol%, the emission intensities of EZO(5) and EZO(10) abruptly increase, which are significantly stronger than that of EZO(1), even though the crystallinity of EZO(5) and EZO(10) is much lower than that of EZO(1) as shown in Fig. 4. Their spectra are composed of two shoulders at 1.554 and 1.580 μm in addition to the main peak at 1.538 μm. As described in XRD data, EZO(5) and EZO(10) exhibited strong Er_2O_3 peaks as well as ZnO peaks. It can be speculated that they are generated from both Er ions incorporated in the ZnO lattice, and those congregated at the intra-grain and/or segregated at the grain boundaries. The latter Er ions are independent of the outside factors such as the crystal field and the induced strain, and so they can be directly pumped by the excitation source, contributing to the high emission intensity dominantly and showing the sharp spectra. Furthermore the shoulder peak at 1.578 μm in EZO(5) and EZO(10), which is not attained in EZO(1) and EZO(3), reveals that this emission is not related to the Er^{3+} ions incorporated in ZnO lattice.

4. Conclusion

ZnO thin films with various Er content were prepared by rf magnetron sputtering. The Er/Zn atomic ratio demonstrated that Er atoms arrived onto the substrates more than Zn atoms due to scattering angle difference in sputtered atoms, which were attributed to the different atomic weights. After post-annealing, the stress of as-deposited films was relaxed and also the atoms were rearranged because of the thermal energy, resulting in the well-developed (0 0 2) preferred orientation at 34.4°, whereas as-deposited films had almost amorphous-like structure. EZO(1) was superior to EZO(3) in IR emission intensity in spite of the low Er content, while the crystallinity of EZO(1) was better than that of EZO(3). This result demonstrated that the higher crystallinity contributed to the enhanced emission more than the higher Er content. The fairly enhanced emissions of EZO(5) and EZO(10) were mainly attributed to Er ions congregated at the intra-grain and/or segregated at the grain boundaries.

Acknowledgments

This research was supported by Basic Science Research Program through the National Research Foundation of Korea (NRF) funded by the Ministry of Education, Science and Technology (no. 313-2008-2-D00435).

References

[1] G. Lakshminarayana, R.V. Sagar, S. Buddhudu, NIR luminescence from Er^{3+}/Yb^{3+}, Tm^{3+}/Yb^{3+}, Er^{3+}/Tm^{3+} and Nd^{3+} ions-doped zincborotellurite glasses for optical amplification, Journal of Luminescence 128 (2008) 690–695.

[2] R.P. Casero, A.G. Llorente, O.P.Y. Moll, W. Seiler, R.M. Defourneau, D. Defourneau, E. Millon, J. Perrière, P. Goldner, B. Viana, Er-doped ZnO thin films grown by pulsed-laser deposition, Journal of Applied Physics 97 (2005) 054905–054908.

[3] R.G. Wilson, R.N. Schwartz, C.R. Abernathly, S.J. Pearton, N. Newman, M. Rubin, T. Fu, J.M. Zavada, 1. 54 μm photoluminescence from Er-implanted GaN and AlN, Applied Physics Letters 65 (1994) 992–994.

[4] K. Takahei, K. Taguchi, Selective formation of an efficient Er–O luminescence center in GaAs by metalorganic chemical vapor deposition under an atmosphere containing oxygen, Journal of Applied Physics 74 (1993) 1979–1982.

[5] A. Polman, Erbium implanted thin film photonic materials, Journal of Applied Physics 82 (1997) 1–39.

[6] S. Komuro, T. Katsumata, T. Morikawa, X. Zhao, H. Isshiki, Y. Aoyagi, 1. 54 μm emission dynamics of erbium doped zinc–oxide thin films, Applied Physics Letters 76 (2000) 3935–3937.

[7] S. Komuro, T. Katsumata, T. Morikawa, X. Zhao, H. Isshiki, Y. Aoyagi, Highly erbium-doped zinc–oxide thin film prepared by laser ablation and its 1.54 μm emission dynamics, Applied Physics Letters 88 (2000) 7129–7136.

[8] M. Ishii, S. Komuro, T. Morikawa, Y. Aoyagi, Local structure analysis of an optically active center in Er-doped ZnO thin film, Journal of Applied Physics 89 (2001) 3679–3684.

[9] M. Ishii, Y. Komukai, Theoretical prediction of local distortion in an ErO_6 cluster: stabilization of a C_{4v} structure by a rack and pinion effect, Applied Physics Letters 79 (2001) 934–936.

[10] Z. Zhou, T. Komori, T. Ayukawa, A. Koizumi, Y. Takeda, Li- and Er-codoped ZnO with enhanced 1.54μm photoemission, Applied Physics Letters 87 (2005) 091109–091113.

[11] H. Song, Y.J. Kim, Characterization of luminescent properties of ZnO:Er thin films prepared by rf magnetron sputtering, Journal of the European Ceramic Society 27 (2007) 3745–3748.

[12] S.M. Chung, S.H. Jan, Y.J. Kim, Characterization of compositional variation and luminescence of $ZnGa_2O_4$:Mn thin film phosphor, Materials Letters 59 (2005) 786–789.

[13] Z.B. Ayadi, L.E. Mir, K. Djessas, S. Alaya, Electrical and optical properties of aluminum-doped zinc oxide sputtered from an aerogel nanopowder target, Nanotechnology 18 (2007) 445702–445706.

[14] J.G. Lu, S. Fujita, T. Kawaharamura, H. Nishinaka, Y. Kamada, T. OhShima, Z.Z. Ye, Y.J. Zeng, Y.Z. Zhang, L.P. He, B.H. Zhao, Carrier concentration dependence of band gap shift in n-type ZnO:Al films, Journal of Applied Physics 101 (2007) 083705–083707.